UDK: 519.673:623.52
COSATI: 19-01, 12-01

Fem Techniques in Shaped Charge Simulation

Marinko Ugrčić, PhD (Eng)[1)]
Dušan Ugrčić, (advanced university student)[2)]

The method of shaped charge simulation based on the FEM techniques is presented. The earlier phases of shaped charge functioning include the initiation of detonation and detonation wave propagating along the explosive charge. After shaped charge jet and slag forming the phases of jet stretching and jet penetration follow.
The coupled FEM based on Eulerian-Lagrangian meshing was used to describe the phases of detonation wave propagating as well as the jet forming and jet stretching. But the Lagrangian meshing was used to describe the jet penetration, as the last phase of shaped charge functioning. During penetration very intensive erosion of jet material appears so that the eroded Lagrangian cells must be removed from the calculation. To correctly calculate the jet penetration, the coefficient of erosion was introduced in the FEM solver. The results of the experimental determination of jet erosion during penetration through a steel obstacle were presented. The examples of FEM simulation and the relevant results of the experimental testing of the 64 mm shaped charge jet forming and penetrating are shown as well.

Key words: **shaped charge, shaped charge jet, jet forming, process simulation, numerical simulation, finite element method.**

Introduction

THE shaped charge effect (Munroe's effect) as a physical phenomenon belongs to the fields of nonlinear mechanics. Regarding large civilian and military uses of the mentioned effect the calculation techniques for predicting shaped charge functioning represent a very important interest in the procedures of shaped charge studying and design.

Actually, there are more different methods for shaped charge simulation, but generally they may be: empirical, analytical, numerical, and coupled as well [1]. Whereas the early work was based on trial-and-error experiments (empirical methods), since the 1970s, hydrocodes have been used with some success to predict how a shaped charge would behave. Defourneaux [1], Zukas [2] and Meyers [3] give excellent summaries of shaped charge applications and analytical models. The numerical simulation of the shaped charge effect, besides the modern software based on the finite elements or/and finite differences codes, can be successfully resolved using the analytical programs based on the hydrodynamic theory.

The program codes BASC [4], HOCC [5], ANACONDA [6], SCAP [7] and HYDRO [8, 9] for the numerical simulation of the shaped charge function and jet penetration, make it possible to calculate more accurately the jet kinematics parameters and its penetrability in the obstacles of different mechanical properties. The mentioned analytical models that describe formation of the jet, its break-up and penetration of target, play an important role in the optimization of shaped charges. A number of such models were developed over the world during last years [10, 11]. The results of Russian development of such an analytic methodology and an example of its application for a shaped charge optimization were presented in [12].

The finite element method (FEM) is also used for numerical simulations of the formation, fragmentation and copper plate penetration of a jet that develops in a shaped charge. Zukas [13] and Camacho [14] describe the computational methodology in greater details giving the focus on jet breakage. Some of more or less known the FEM numerical codes are: HELP, EPIC, HEMP, PISCES [15], DYNA [16, 17], AUTODYN, LS-DYNA, CATIA, etc.

Besides verifying the FEM as a predictive technique, the main aims of the paper include:

- Mathematical modelling of the shaped charge functioning with additional assumptions such as propagating of detonation wave, collapsing model, jet erosion model, etc., all to upgrade the quality and accuracy of computing;
- Numerical simulation of the shaped charge functioning based on the FEM techniques in the way to verify the method for predicting shaped charge mechanisms; and
- Evaluation of the FEM techniques by comparing the computed and experimental results.

System of constitutive equations

The partial differential equations express the conservation of mass, momentum and energy in the Lagrangian coordinates. These, together with the equations of state (material models) [18] and a set of initial and boundary conditions, define the complete solution of the problem. Material continuum associated with a Lagrangian zone stays with that zone under any deformation. Thus a

[1)] Military Academy,Pavla Jurišića Šturma 33, 11000 Belgrade, SERBIA
[2)] Faculty of Mechanical Engineering, University of Belgrade, Kraljice Marije 16, 11000 Belgrade, SERBIA

Lagrangian grid moves and distorts during time with the material automatically satisfying the **conservation of mass**. The density ρ at any time can be determined from the current volume V of the zone and its initial mass m

$$\rho = \frac{\rho_0 V_0}{V} = \frac{m}{V} \tag{1}$$

where is: ρ_0 – initial density and V_0 – initial volume. Then, the partial differential equations which express the **conservation of momentum** relate the acceleration and stress tensor σ_{ij}

$$\rho\ddot{x} = \frac{\partial \sigma_{xx}}{\partial x} + \frac{\partial \sigma_{xy}}{\partial y} + \frac{\partial \sigma_{xz}}{\partial z}$$

$$\rho\ddot{y} = \frac{\partial \sigma_{yx}}{\partial x} + \frac{\partial \sigma_{yy}}{\partial y} + \frac{\partial \sigma_{yz}}{\partial z}$$

$$\rho\ddot{z} = \frac{\partial \sigma_{zx}}{\partial x} + \frac{\partial \sigma_{zy}}{\partial y} + \frac{\partial \sigma_{zz}}{\partial z}\,. \tag{2}$$

where is: $\ddot{x}, \ddot{y}, \ddot{z}$ – components of the vector of acceleration. Here it is necessary to emphasise that the **stress tensor** is separated into a hydrostatic component p with the artificial viscosity q and the deviatoric component s_{ij} that is discussed more largely in [18].

$$\sigma_{xx} = -(p+q) + s_{xx}$$

$$\sigma_{yy} = -(p+q) + s_{yy}$$

$$\sigma_{zz} = -(p+q) + s_{zz}$$

$$\sigma_{xy} = s_{xy}$$

$$\sigma_{yz} = s_{yz}$$

$$\sigma_{zx} = s_{zx}\,. \tag{3}$$

The negative sign for the hydrostatic pressure p follows from the usual notion that stresses are positive in tension and negative in compression (the opposite to that for pressure). In the above mentioned equations the hydrostatic pressure p is an argument by the pseudo-viscous force q which is discussed more fully in [18].

The **strain tensor** ε_{ij} is determined from the relation between the strain rates and the velocities ($\dot{x}, \dot{y}, \dot{z}$)

$$\dot{\varepsilon}_{xx} = \frac{\partial \dot{x}}{\partial x}$$

$$\dot{\varepsilon}_{yy} = \frac{\partial \dot{y}}{\partial y}$$

$$\dot{\varepsilon}_{zz} = \frac{\partial \dot{z}}{\partial z}$$

$$\dot{\varepsilon}_{xy} = \frac{1}{2}\left(\frac{\partial \dot{x}}{\partial y} + \frac{\partial \dot{y}}{\partial x}\right)$$

$$\dot{\varepsilon}_{yx} = \frac{1}{2}\left(\frac{\partial \dot{y}}{\partial z} + \frac{\partial \dot{z}}{\partial y}\right)$$

$$\dot{\varepsilon}_{zx} = \frac{1}{2}\left(\frac{\partial \dot{z}}{\partial x} + \frac{\partial \dot{x}}{\partial z}\right). \tag{4}$$

These strain rates are related to the rate of the change of the volume $\frac{\dot{V}}{V}$ by

$$\frac{\dot{V}}{V} = \dot{\varepsilon}_{xx} + \dot{\varepsilon}_{yy} + \dot{\varepsilon}_{zz}\,. \tag{5}$$

Elastic flow region. For the elastic behaviour of a material determined by derivation of Eq. (5) and Hook's Law relations between the deviatoric stress rates and the strain rates

$$\dot{s}_{xx} = 2G\left(\dot{\varepsilon}_{xx} - \frac{1}{3}\frac{\dot{V}}{V}\right)$$

$$\dot{s}_{yy} = 2G\left(\dot{\varepsilon}_{yy} - \frac{1}{3}\frac{\dot{V}}{V}\right)$$

$$\dot{s}_{zz} = 2G\left(\dot{\varepsilon}_{zz} - \frac{1}{3}\frac{\dot{V}}{V}\right)$$

$$\dot{s}_{xy} = 2G\dot{\varepsilon}_{xy}$$

$$\dot{s}_{yz} = 2G\dot{\varepsilon}_{yz}$$

$$\dot{s}_{zx} = 2G\dot{\varepsilon}_{zx}\,. \tag{6}$$

where is: G – shear modulus. The deviatoric variables will also be adjusted for other real effects, such as rigid body rotations, plastic flow, damage and failure as described in detail in [18, 19].

Plastic flow region. A pragmatic approach in the choice of criterion for yield criteria has involved in use the **Von Mises yield criterion** (used in most hydrocodes as well) to describe the elastic limit and transition to the plastic flow. This applied criterion provide a relatively smooth and continuous yield surface. The state that, given the principal stresses σ_1, σ_2 and σ_3, the local yield condition is

$$(\sigma_1 - \sigma_2)^2 + (\sigma_2 - \sigma_3)^2 + (\sigma_3 - \sigma_1)^2 = 2Y \tag{7}$$

where is: Y – the yield strength in simple tension.

Equations of state. The pressure p is related to the density ρ and specific internal energy e through the equation of state given in general form

$$p = f(\rho, e) \tag{8}$$

Different forms of the state equations are described in [18]. This must be solved simultaneously with the equation expressing the conservation of energy

$$\dot{e} = \frac{1}{\rho}(\sigma_{xx}\dot{\varepsilon}_{xx} + \sigma_{yy}\dot{\varepsilon}_{yy} + \sigma_{zz}\dot{\varepsilon}_{zz} + 2\sigma_{xy}\dot{\varepsilon}_{xy} + 2\sigma_{yz}\dot{\varepsilon}_{yz} + 2\sigma_{zx}\dot{\varepsilon}_{zx}). \tag{9}$$

Finally, several types of equations to define the state of gaseous products of detonation are involved in mathematical modelling, e.g. **Becker-Kistiakowsky-Wilson (BKW) equation** or frequently **Jones-Wilkins-Lee (JWL) equation** given in the form:

$$p = A\left(1-\frac{\omega\eta}{R_1}\right)e^{-\frac{R_1}{\eta}} + B\left(1-\frac{\omega\eta}{R_2}\right)e^{-\frac{R_2}{\eta}} + e\omega\eta\,. \quad (10)$$

where is: $\eta=\rho/\rho_e$ – ratio of density of detonation products and explosive charge and e – energy of detonation per volume unit. The values of constants A, R_1, B, R_2, and ω for very common explosives have been determined from dynamic experiments and are available for solver users in the relevant material library.

Mathematical models used in the solver

The phenomena associated with shaped charges include high explosive detonation and extreme deformations of the shaped charge casing and liner present a challenging task for the numerical analysis.

The solver provides the analyst with a number of different options for shaped charge design. These options range from using a highly efficient **jetting option** to the use of the full Euler/Lagrange processor capabilities within the program. The jetting option, discussed in [18], uses a **combined numerical and analytical approach**. Two-dimensional finite difference Euler grids represent components such as the explosive, liner and waveshaper, while Lagrange grids model the casings, fuze and other thin components of shaped charge. For the liner, modelled as a thin Euler grid, an additional analytic jetting option is invoked which allows the liner to behave as a shaped charge jet and slug.

In order to achieve better calculating accuracy the mathematical model was improved. The first improvement relates to the erosion model during jet penetration and the second one to the jet analysis (liner collapsing and jet and slug forming).

Erosion model

Although the solver can calculate with both Lagrangian and Eulerian grids, it may sometimes be the case that materials have to be defined using Lagrangian grids even though it is clear that these materials will be subjected to very large distortions arising from intensive motion of the Lagrange grid.

For example, this is the case of jet and projectile penetration through an obstacle. In the cases of jet and projectile penetration the target and "penetrator" materials in hypervelocity impact problems will be subject to gross distortion and again an accurate calculation of this problem should follow the material as it "splashes".

When an eroded cell is removed from the calculation process in this way, the mass within the cell can either be discarded or distributed to the corner nodes of the cell. If the mass is retained, conservation of inertia and spatial continuity of inertia are maintained. However the compressive strength and internal energy of the material within the cell are lost whether or not the mass is retained. This discard procedure is known as **erosion**. However it is important to note that, in general, this is not true modelling of a physical phenomenon, but a numerical palliative introduced to overcome the problems associated with the mesh distortions caused by gross motions of a Lagrangian grid.

Because of the losses of internal energy, strength and (possibly) mass, care must be taken in using this option and erosion strain limits chosen wisely so that cells are not discarded (eroded) until they are severely deformed and their compressive strength and/or mass are not likely to affect the overall results.

Fig.1 illustrates clearly the effect of the values of the limiting erosion strains on the final crater dimensions in a hypervelocity impact problem [18].

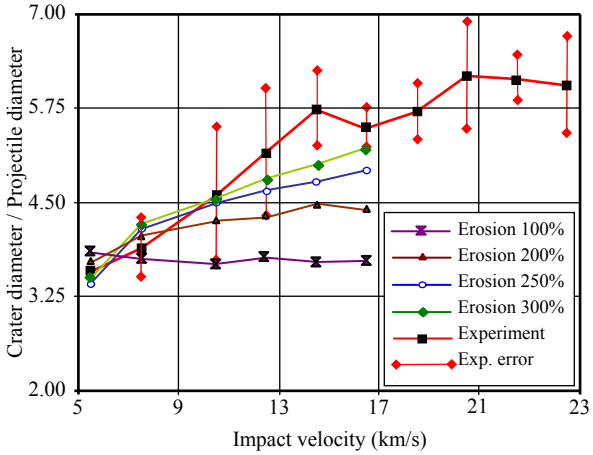

Figure 1. Comparison of the experimental crater dimensions and the AUTODYN results for different erosion strains

In this problem maximum erosion strains of 300% or higher are appropriate but it should be noted that these were geometric strains and different values might be more appropriate if effective plastic strains were being tested.

In the case of the shaped charge functioning, the jet erosion strain was determined on the basis of the theoretical and experimental method given in [20]. As the rate of jet erosion we can express principally as a ratio of the jet velocity v_{jet} and the velocity of jet penetration u_x (v_{jet}/v_{jet}-u_x), so that using the relevant curves represented in [20] we can get the appropriate functional dependence given in Fig. 2. The jet erosion example, used in this paper, is based on testing a 64 mm shaped charge model [9, 20].

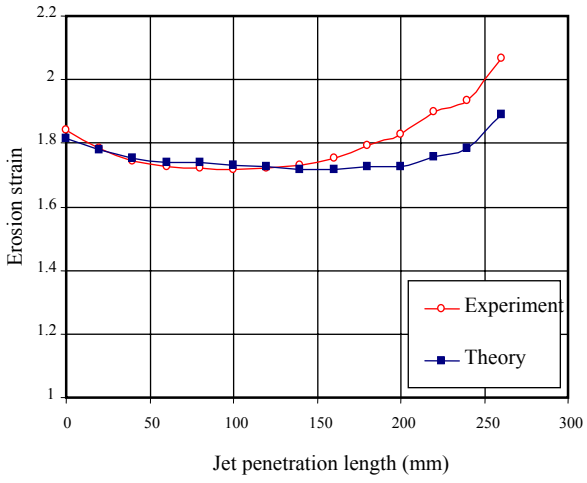

Figure 2. Comparison of theoretical and experimental jet erosion strains in a steel obstacle

According to the diagrams of theoretical and experimental jet erosion strains (Fig.2), erosion of the jet during penetration through a steel obstacle takes the values between 172 and 207%. Similar values of the jet erosion rate appear in the cases of penetration through other types of material, for example concrete, ceramics, glass, etc.

Jetting analysis

A two-dimensional Eulerian grid is used to model the liner. By definition, this avoids any mesh distortion. To accurately perform such an analysis using Euler requires a

large, finely zoned mesh. In the jetting option the liner is modelled like an explosive part with full Euler detail. In this way, the full hydrodynamic equations of motion are used to compute the collapse velocity and the collapse angle for each liner mass point.

These values are used in conjunction with an analytic jet formation algorithm to obtain the jet and slug masses and associated velocities. An optional jetting analysis has been included in the solver which uses post calculation values to provide an improved estimate of the collapse angle β and the relevant jetting parameters depending on this angle.

The following diagram (Fig.3) shows the vector triangle formed by the collapse velocity v_0, the velocity v_C of the stagnation point C and the velocity v_r of the jet (relative to the stagnation point C).

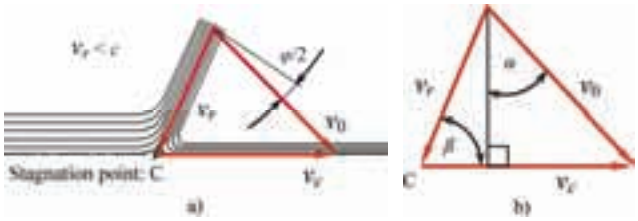

Figure 3. Liner collapsing: a) vector triangle formed by the collapse velocity with the stagnation point; b) velocities triangle in the coordinate system relative to the point C

The velocities v_C and v_r expressed depending on v_{jet} and v_{slug} are

$$v_C = \frac{v_{jet} + v_{slug}}{2} \tag{11}$$

$$v_r = \frac{v_{jet} - v_{slug}}{2}. \tag{12}$$

From the triangle (Fig.3a) the following relationship is obtained

$$\tan(\beta) = \frac{v_0 \cos\alpha}{v_C - v_0 \sin\alpha}. \tag{13}$$

The optional jetting analysis uses the fact that once a calculation is complete, the locus of the stagnation point is defined by the values of (r_{jet}, x_{jet}) obtained for each jetted point and thus v_C can be obtained by differentiating this curve. The differentiation is performed by constructing (fitting) a quadratic polynomial function through points noted by j-1, j and j+1 and taking the derivative at the point j. With v_C known, the above equation can be used to obtain new estimates for the collapse angle β.

Numerical simulation

A possibility of computing code in the tasks of numerical simulation of shaped charge functioning, specially for liner collapsing and jet and slug forming with further jet evolution (jetting) as well as the jet penetration in the steel obstacle will be illustrated.

Mathematical model

For numerical studying a sample of an experimental 64 mm shaped charge model is treated. The axial cross-section of the shaped charge is illustrated in Fig.4.

The main geometrical and physical parameters of the shaped charge are as follows: Explosive charge (octol, density 1.72 g/cm^3), Detonator (pentryte, density 1.61 g/cm^3), Metallic liner (copper, density 8.93 g/cm^3), Angle of the metallic liner cone (inner 50º, outer 51º), Metallic liner apex radius 8.5 mm, Thickness of the metallic liner (progressive, min. thickness 1.0 mm), Metallic body (duralumin, density 2.75 g/cm^3), Thickness of the metallic body (1.5 mm), Waveshaper (teflon, density 2.15 g/cm^3), Stand-off (3 calibres).

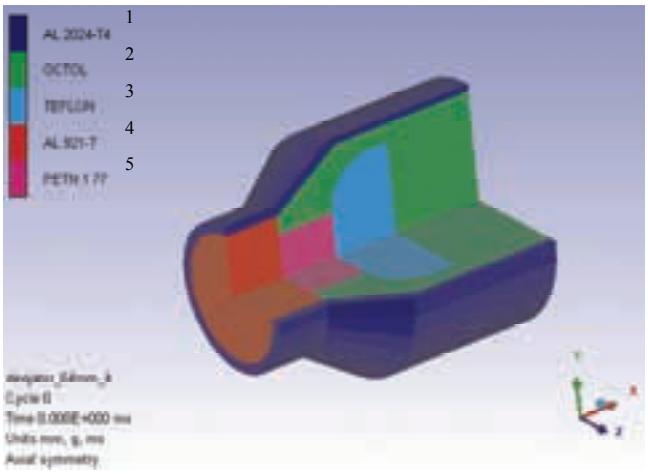

Figure 4. Axial cross-section of 64 mm shaped charge 3D model
1.- Casing; 2.- Explosive charge; 3.- Waveshaper; 4.- Fuze; 5.- Detnator

The Fig.5 illustrates the initial coupled Lagrange-Euler meshing of the shaped charge given in the pre-processing procedure.

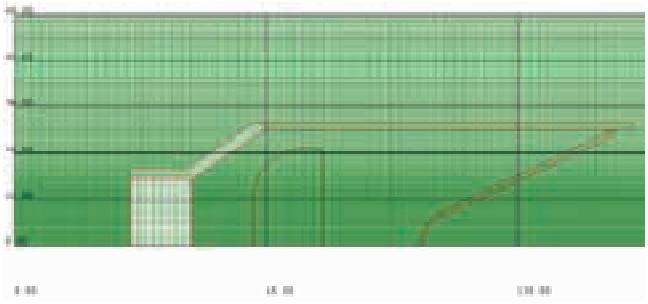

Figure 5. Coupled Lagrange-Euler meshing of the 64 mm shaped charge model (axial half-section)

The Euler mesh was generated by the use of changeable cells of dimensions: from 1×1 mm on the peripheral zone till 0.25×0.25 mm near to the symmetry axis of the shaped charge.

Detonation wave propagation

The numerical analysis of the interaction of a detonation wave and the waveshaper as well as the solving of its optimization is carried out successfully using a computer software based on the method of finite differences and/or finite elements.

To model the process of detonating high explosive in the FEM it is usual to use the **burn on time** option [18].

In its ideal form this assumes that, on initiation, a detonation wave travels away from the initiation point with constant detonation velocity, being refracted around any inert obstacles in the explosive without moving the obstacle, maintaining a constant detonation velocity in the refracted zone and detonating each particle of explosive on arrival at that particle.

Thus for a system such as that illustrated in Fig.6, where an inert obstacle lies within a slab of explosive which is initiated at one end, the detonation wave travels radially

away from the initiation point until it meets the obstacle, then travels around the obstacle and travels on, being refracted within the "shadow zone" of the explosive which lies behind the obstacle i.e. below the tangent OX.

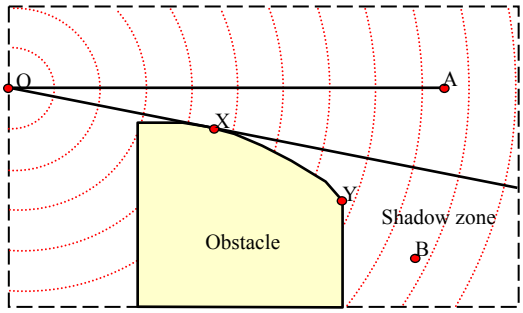

Figure 6. Transit of a detonation wave around an inert obstacle

For each cell in the initial computing mesh in the high explosive, the values for the arrival time of the detonation wave at the cell and the transit time across the cell (based on the cell area and diagonals to avoid directional variations) are calculated from the input detonation velocity.

The true arrival time at a given cell is that along the shortest path from the initiation point (or plane, or circle) to the nearest corner of the cell, taking full account of inert obstacles which may be in the path of the detonation wave, and the wave is assumed to travel with constant velocity equal to the predefined value of the detonation velocity *D*.

However, in the above figure, while it is a simple matter to determine the arrival time at a point such as A, being OA/*D*, to determine the arrival time at a point such as B it is necessary to determine the distance OX, together with the distance YB, the distance from B along its tangent to the obstacle and also the arc length XY along the obstacle values of YB and XY vary for all points in the "shadow zone". Thus the determination of the arrival times of all points in the "shadow zone" would require very extensive and time-consuming calculations.

Fig.7 illustrates the regions of influence of two initiation points O_1 and O_2. In each region of influence the detonation wave radiates away freely from the initiation point so that the arrival time from that point is simply calculated. Then for the points X_1, X_2, X_3 and X_4 as typical points within the explosive, if $T(X)$ is the "burn time" (i.e. the arrival time of the detonation wave) at the point "X", then:

- $T(X_1) = O_1X_1 / D$;
- $T(X_2) = O_1O_2 / D + O_2X_2 / D$; and
- $T(X_3) = \min [O_1X_3; O_1O_2 + O_2X_3] / D = O_1X_3 / D$ (even though X_3 is within the region of influence of O_2).

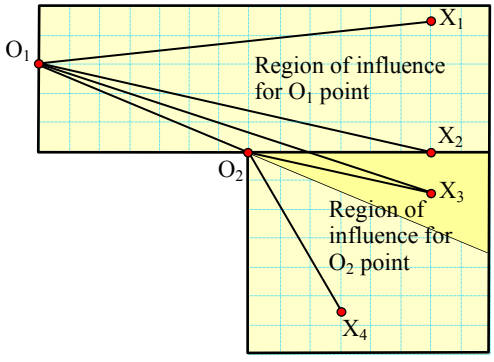

Figure 7. Regions of influence of the initiation points

Figures 8 - 11 illustrate the initial meshing and the most important details of interaction of the detonation wave and the waveshaper given by the numerical simulation. The results consider the experimental model of the initiation and detonation device of the 64 mm shaped charge.

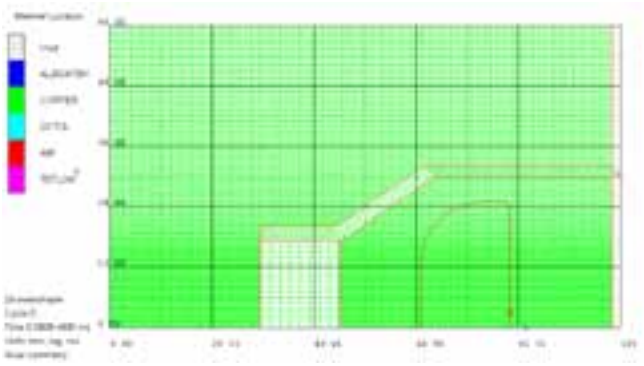

Figure 8. – Initial meshing of 2D modeled parts to describe detonation wave propagating

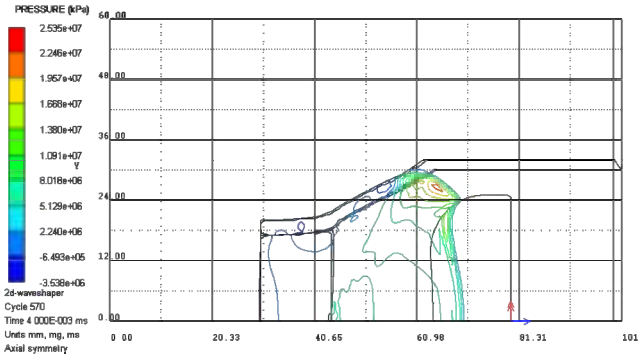

Figure 9. – Detonation wave passing around the frontal side of the waveshaper

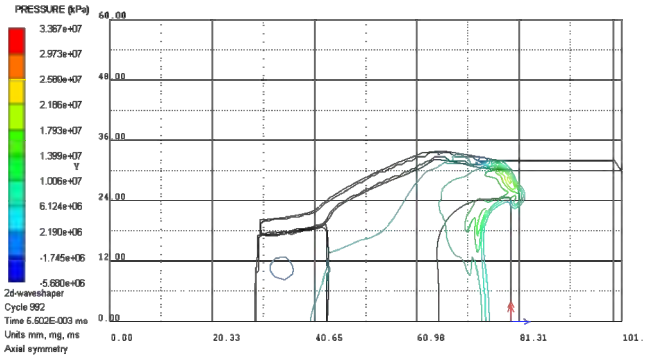

Figure 10. – Detonation wave transferring trough the contact surface

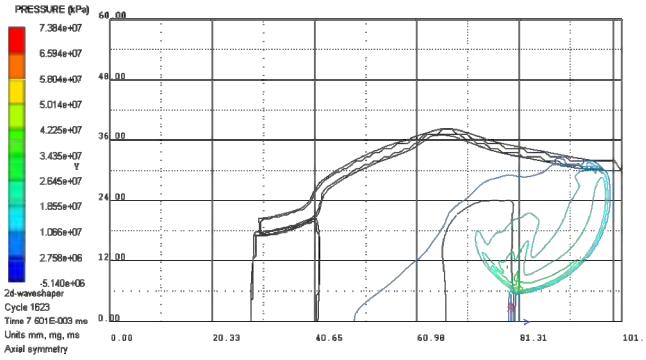

Figure 11. – Detonation wave passing around the end side of the waveshaper

Coupled Eulerian and Lagrangian meshing is used. So, the Eulerian meshing is used to make the model of the ambient air and for modeling the explosive and the waveshaper as well and the Lagrangian meshing is used for modeling the casing and the fuze.

Modeling energy release in high explosives

Fractions of the chemical energy Q are fed in as energy inputs to the cell at appropriate times so that by the time the detonation has swept across the cell, all the chemical energy has been input and the explosive within that cell has completely detonated [18]. The explosive is then assumed to be detonation products and its (p,v) state to lie on the CJ adiabate.

However since the shock has not been infinitely thin (since finite burn times and shock capturing techniques are used in the solver) it is not to be expected that the pressure will reach the theoretical CJ value during this detonation process. The path followed by a typical cell in the (p,v) plane will be similar to that shown in Fig.12. The permitted total energy error involved in the explosive system is up to 5% of the released high explosive chemical energy Q.

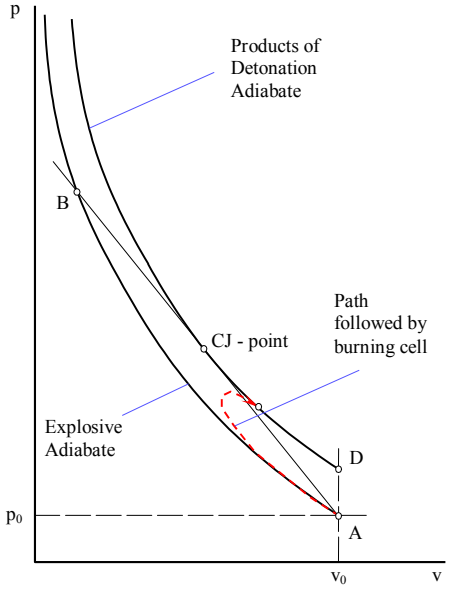

Figure 12. Path followed in the (p,v) plane by the burning cell

If the initiation time for a detonation point is not specified, it will be automatically determined from the initiation and transit times from other points, whose initiation times have been specified or determined in the same fashion. Clearly, at least one detonation point must have its initiation time specified.

This is a recommended method for modeling detonation around objects if the best accuracy is required.

Particles velocities

One of interesting details relative to the shaped charge functioning considers a field of particle velocities, especially in the zone of gaseous products of detonation, then metallic liner collapsing and casing rejecting.

Of course, the particle velocities of jet elements are of primordial interest.

Based on the calculated picture of particle velocities, the determination of active mass is possible. The active mass represents a part of the whole explosive charge the detonation products of which are oriented to the metallic liner.

This mass is determined by the line of collision (contour surface in the space) two decompression waves propagating from the free surfaces of the explosive charge (Fig.13, line a and zone A).

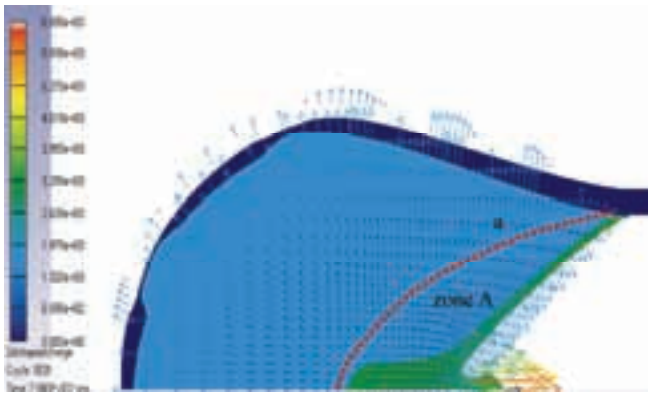

Figure 13. Particles velocities and active mass of the shaped charge (given by FEM)

Jetting

Jet and slug formation as well as the further jet evolution (jetting) given by computing are illustrated in Fig.14. The shown frames are related to the sequences of 19 μs, 24 μs and 27 μs (from the left to the right, respectively) from the shaped charge initiation.

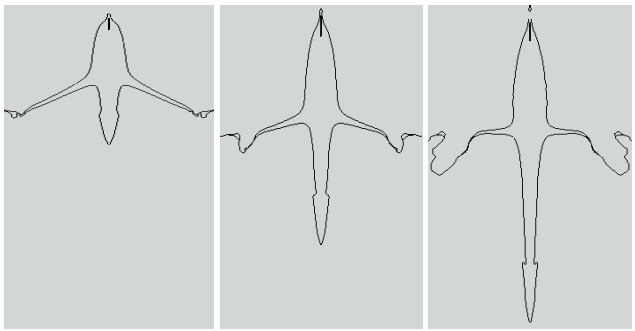

Figure 14. Shaped charge jet forming and stretching (numerical simulation)

Jet penetration

The jet penetration through the obstacle is described by the hydrodynamic theory of the shaped charge. According to this theory, the mechanical characteristics of the jet material and the obstacle material concerning the mechanical resistance are neglected in the first phases of the penetrating process.

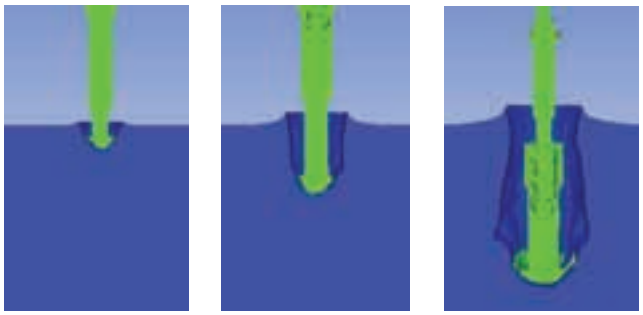

Figure 15. Jet penetration through the steel obstacle (numerical simulation)

Fig.15 shows the penetration of the 64 mm shaped charge model copper jet through a steel obstacle. The jet

moves with $v_{jet} \approx 8000$ m/s tip velocity. The pictures given by the numerical simulation nicely clarify the process of the jet penetrating phenomenon.

Experimental results

In the order to estimate the quality of the results given by numerical simulation there are presented some relevant results of the experimental testing of the 64 mm calibre shaped charge model. The method of impulse radiography and the radiograph equipment SCANDIFLASH 600 kV - type were used to make the radiographs illustrated in Figures 16 and 17.

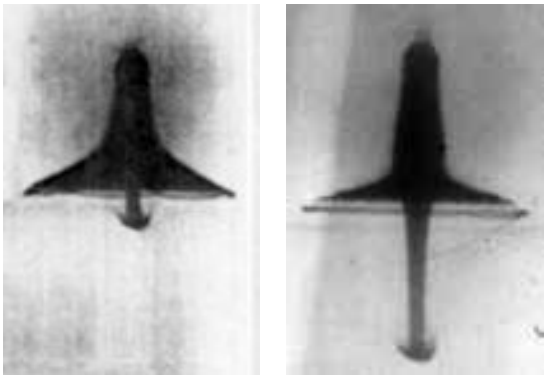

Figure 16. Radiographs of jet formation and stretching

Fig.16 illustrates the jetting (liner collapsing and jet formation with stretching) of the 64 mm calibre shaped charge model at the moment of 18.6 μs and 23.6 μs after charge activation. The measured jet tip velocity in the final stage of forming is about 8000 m/s.

Fig.17 shows the penetration of the copper penetrator moving with a velocity $v_{jet} = 1250$ m/s through a duralumin obstacle. The radiographs are given by the use of the techniques of Kino-radiography.

The radiographs in Fig.17 are used to qualitatively compare numerical and experimental results only.

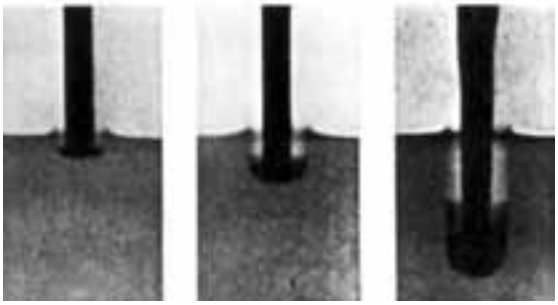

Figure 17. Jet penetration through a duralumin target (radiographs)

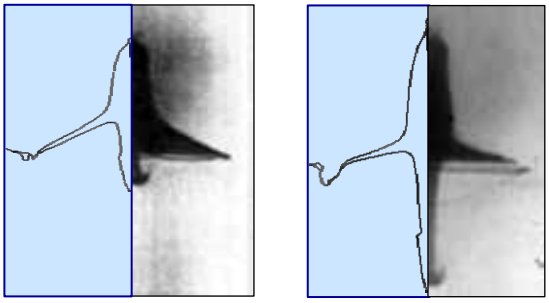

Figure 18. Comparing of testing and computing results at the moment the 18.6 μs (left) and 23.6 μs (right) the after explosive charge activation (left half-sketches are given by the numerical simulation and right half-radiographs are given by the X-ray technique)

Finally, to the confirm advantages of the presented predicting FEM techniques, the comparative sequences of the liner collapsing and the further jetting given by the computing and the experiment are illustrated in Fig.18.

Conclusion

Summarising the results of the study given in the paper, we can draw the main conclusions as follows:

- Mathematical modelling of the shaped charge functioning with involved additional assumptions relative to the propagating of detonation wave, collapsing model, jet erosion model and modeling energy release in high explosives was carried out successfully. The main contribution in this part represents the rate of jet erosion determined experimentally by an original procedure;
- Numerical simulation of the shaped charge functioning based on the coupled Eulerian and Lagrangian FEM techniques was verified. The presented method is a powerful tool for predicting shaped charge mechanisms; and
- Evaluation of the FEM techniques by comparing the computed and experimental results showed very high and multilevel benefit of the used predictive techniques. The comparative analysis of the computed and the experimental results does not show considerable discrepancies. The overlapping between the results of numerical modelling and the experimental data on the parameters such as the jet and slug velocity and their geometry is very good. So, the numerical simulation by the given FEM technique represents the best way to predicts the parameters of shaped charge functioning.

References

[1] DEFOURNEAUX,M.: *La Simulation Numérique des Charges Creuses*, Sciences et Techniques de l'Armement, 51, 3e fasc., Paris, 1977.

[2] ZUKAS,J.A.: *High-Velocity Impact Dynamics*, Wiley, New York, 1990.

[3] MEYERS,M.A.: *Dynamic Behaviour of Materials*, Wiley, New York, 1994.

[4] HARRISON,J.T.: *BASC, An Analytical Code for Calculating Shaped Charge Properties*, 6. International Symposium on Ballistics, Orlando – USA, 1981.

[5] DEFOURNEAUX,M.: *Organisation d'un Programme Analytique pour le Calcul des Charges Creuses*, Sciences et Techniques de l'Armement, 51, 4e fasc., Paris, 1977.

[6] NICHOLSON,J.S. et all.: *A Simple Model for Predicting Shaped Charge Jet Lateral Velocity Vectors Resulting From Asymmetric Liner Collapse*, 11. International Symposium on Ballistics, Brusseles –Belgium, 1989.

[7] VIGIL,M.G.: *Optimized Conical Shaped Charge Design Using the SCAP Code*, Scandia National Laboratories, Albuquerque – Livermore, 1988.

[8] UGRČIĆ,M.: *Numerical Simulation and Optimisation of the Shaped Charge Function*, Naučnotehnički pregled, Belgrade, 1998, Vol.XLVIII, No.4, pp.30-41.

[9] UGRČIĆ,M.: *Determination of the Critical Jet Velocity During the Penetration into the Homogenous Steel Obstacle*, Series Mech., Aut. Control, and Robotics, Facta universitatis, Niš, 2003, Vol.3, No.15, pp.981-988.

[10] ARLOW,A.J., CURTIS,J.P.: *Analytic Computer Models for the Design and Evaluation of Shaped Charges*, Proc. The 15th Int. Symp. Ballistics, Vol.2, Jerusalem, Israel, 1995, pp. WM/211-218.

[11] SOFRONOV,I.D., et all.: *Calculation of Shaped Charge Performance*, Proc. Int. Seminar on Fundamental Problems of Cumulation, St. Petersburg, Russia, 1997, pp.230-259.

[12] SWIRSKY,O.V., et all.: *The Analytical Model ATOS-M for Computing of the Shaped Charge Jet Penetration Parameters*, Int. J. Impact Engineering, 29, 2003, pp.683-690.

[13] WALTERS,W.P., ZUKAS,J.A.: *Fundamentals of Shaped Charges,* A Wiley-Interscience Publication, John Wiley and sons, New York, 1989.

[14] CAMACHO,G., ORTIZ,M.: *Adaptive Lagrangian Modelling of Ballistic Penetration of Metallic Targets*, Comput. Methods Appl. Mech. Eng. 142, 1997, pp.269–301.

[15] Physics International Company: *PISCES 2D ELK, A Code to Solve Dynamic Fluidflow Structural and Fluid-Structures Interaction Problems*, Prospects, USA, 1988.

[16] HALLQUIST,J.O.: *User's Manual for DYNA 2D. An Explicit Two-Dimensional Hydrodynamic Finite Element Code with Interactive Rezoning*, LLNL Report, USA, 1988.

[17] HALLQUIST,J.O.: *DYNA3D USER'S MANUAL - Nonlinear Dynamic Analysis of Solids in Three Dimensions*, LLNL Report, USA, 1984.

[18] www.century-dynamics.com and www.ansys.com *Theory manual*, Century Dynamics, Solutions through Software, Huston, USA

[19] TEMAM,R., MIRANVILLE,A.: *Mathematical Modeling In Continuum Mechanics*, Second edition, Cambridge University Press The Edinburgh Building, Cambridge UK, Published in the United States of America by Cambridge University Press, New York, 2005.

[20] UGRČIĆ,M., VUKAŠINOVIĆ,M.: *Determination of Main Parameters of Jet Penetration into the Homogenous Steel Obstacle*, Scientific Technical Review, Belgrade, 2003, Vol.LII, No.5-6, pp.3-9.

Received: 15.01.2009.

Primena metoda konačnih elemenata u simulaciji kumulativnog punjenja

Prikazan je postupak simulacije kumulativnog punjenja baziran na metodama konačnih elemenata. Početne faze funkcije kumulativnog punjenja podrazumevaju iniciranje detonacije i širenje detonacionog talasa kroz eksplozivno punjenje. Nakon formiranja primarnog u sekundarnog kumulativnog mlaza proces se nastavlja fazama izduženja i prodiranja mlaza.

Kuplovana metoda konačnih elemenata, zasnovana na kombinovanju Ojler-Laganžove mreže konačnih elemenata, korišćena je za opisivanje faza širenja detonacionog talasa kao i formiranja i izduženja mlaza. Lagranžova mreža je korišćena za opisivanje prodiranja mlaza, kao zadnje faze funkcije kumulativnog punjenja. Tokom prodiranja javlja se veoma intenzivna erozija materijala mlaza, tako da se erodirani Lagranžovi elementi moraju isključiti iz predračuna. Za korektan proračun prodiranja mlaza, u solver je uveden koeficijent erozije. Prikazani su rezultati eksperimentalnog određivanja erozije mlaza tokom prodiranja kroz prepreku. Takođe, prokazani su i primeri simulacije dobijeni metodom konačnih elemenata i relevantni rezultati eksperimentalnog ispitivanja formiranja i prodiranja mlaza modela kumulativnog punjenja 64 mm.

Ključne reči: **kumulativno punjenje, kumulativni mlaz, formiranje mlaza, simulacija procesa, numerička simulacija i metoda konačnih elemenata.**

Применение метода конечных элементов в моделировании кумулятивного заряда

В настоящей работе показан способ моделирования кумулятивного заряда, обоснован на методах конечных элементов. Начальные фазы функции кумулятивного заряда подразумевают инициирующие детонации и расширение детонационной волны через взрывчатый заряд. После формирования первычной и вторичной кумулятивной струи процесс продолжается через фазы удлинения и проникновения струи.

Сцепной метод конечных элементов, обоснован на комбинировании сети Ойлер-Лагранжа конечных элементов, использован для описывания фазы расширения детонационной волны, а в том числе и для формирования и продлинения струи. Сеть Лагранжа пользована для описывания проникновения струи в роли последней фазы функции кумулятивного заряда. В течении проникновения струи является очень интенсивная эрозия материала струи, иза-за чего эродированные элементы Лагранжа нужно выключить из расчёта. Ради корректного расчёта проникновения струи в солвер (решающее устройство) введён коэффициент эрозии. Здесь показаны результаты экспериментального определения эрозии струи в течении проникновения через препятствие. А также показаны и примеры моделирования, получены методом конечных элементов и существенные результаты экспериментального исследования формирования и проникновения струи модели кумулятивного заряда 64 мм.

Ключевые слова: **кумулятивный заряд, кумулятивная струя, формирование струи, моделирование процесса, цифровое моделирование, метод конечных элементов.**

Application de la méthode des éléments finis dans la simulation de la charge creuse

Le procédé de la simulation de la charge creuse basé sur la méthode des éléments finis a été présenté dans le cadre de cet article. Les phases initiales de la fonction de charge creuse comprennent l'initiation de la détonation et la propagation de l'onde de détonation à travers la charge explosive. Après la formation du jet primaire en jet secondaire cumulatif, le procédé continue par les phrases d'allongement et de pénétration du jet. La méthode des éléments finis couplée, basée sur la combinaison des réseaux des éléments finis d'Euler-Lagrange est utilisée pour la description de la phase de propagation de l'onde de détonation ainsi que pour la formation et l'allongement du jet. Le réseau de Lagrange est employée pour la description de la pénétration du jet. C'est la dernière phase de la fonction pour la charge creuse. Pendant la pénétration une érosion très intense du matériel se produit de sorte que les éléments érodés de Lagrange sont à exclure du calcul. Pour le calcul correct de la pénétration du jet on a introduit le coefficient d'érosion dans le solver. On a présenté les résultats de la détermination expérimentale de l'érosion du jet lors de la pénétration à travers l'obstacle. Les exemples de la simulation obtenus par la méthode des éléments finis ainsi que les résultats significatifs des essais expérimentaux pour la formation et la pénétration du jet chez le modèle de la charge creuse de 64mm sont présentés aussi.

Mots clés: **charge creuse, jet de la charge creuse, formation du jet, simulation du procédé, simulation numérique, méthode des éléments finis.**